

# Anharmonicity effects in Cu-doped ZnO nanocombs by temperature-dependent Raman scattering

J. F. Kong<sup>1</sup> · D. H. Fan<sup>2</sup> · W. Z. Shen<sup>3</sup>

Received: 8 April 2016 / Accepted: 5 August 2016 / Published online: 11 August 2016  
© Springer-Verlag Berlin Heidelberg 2016

**Abstract** Micro-Raman spectra of  $E_2(\text{high})$  phonon mode in Cu-doped ZnO nanocombs have been presented in detail with different Cu compositions under the temperature ranging from 83 to 443 K grown by a simple catalyst-free chemical vapor deposition method. The alloy disorder effect has been investigated by analyzing the asymmetric broadening of  $E_2(\text{high})$  phonon mode and Cu-induced localized vibration mode at room temperature. In addition, we resort to a theory model including the lattice thermal expansion and anharmonic phonon–phonon interaction, which can well describe the temperature dependence of Raman shift and linewidth of  $E_2(\text{high})$  phonon. In combining with the theory model, we have revealed an increasing anharmonic effect on the Raman shift and linewidth behaviors with increasing Cu composition. Furthermore, it is found that the lifetime of  $E_2(\text{high})$  phonon mode shortens with enhancing the anharmonicity.

## 1 Introduction

Recently, considerable attention has been paid to diluted magnetic semiconductors (DMSs) for exploiting spin in magnetic materials along with the charge of electrons for application in “spintronic” devices [1]. Among the transition-metal-doped ZnO DMSs, both theoretical and experimental investigations have shown that Cu can be used as a p-type dopant in the natural n-type ZnO [2, 3]. Therefore, recent experimental work mainly focuses on the growth of thin films [4, 5] or nanostructures [6, 7] of Cu-doped ZnO by a variety of methods, and accordingly the analysis on the magnetic characterization with the emphasis on the origin of the ferromagnetic behavior in Cu-doped ZnO. Another important fact is that doping Cu ion in ZnO can significantly alter its chemical, electrical, and optical properties [8]. One of the most important aspects of substitutional semiconductor alloys is the nature of the alloy potential fluctuations. Therefore, it is necessary to further understand the lattice dynamical properties in Cu-doped ZnO [6].

As a fast and contactless probe of the lattice vibration in semiconductors, Raman scattering can provide a great deal of information about the phonon vibrations in the center of the Brillouin zone [9]. In ternary semiconductor alloys, Raman spectra of phonon modes, including an asymmetry linewidth broadening, Raman frequency shift, and an emergence of disorder-activated modes, will change with compositional disorder. The detailed information on lattice dynamics can be obtained via observing the parameters of Raman phonon mode, such as Raman frequency, linewidth, and lifetime [10–12]. Additionally, the Raman scattering is also greatly sensitive to the lattice temperature. It is very important to study the evolution of these parameters with temperature for practical applications of ternary alloys

✉ J. F. Kong  
jfkong@sit.edu.cn

✉ D. H. Fan  
donghua\_fan@126.com

<sup>1</sup> School of science, Shanghai Institute of Technology, 100 Hai Quan Road, Fengxian District, Shanghai 201418, People’s Republic of China

<sup>2</sup> School of Applied Physics and Materials, Wuyi University, 22 Dongcheng Village, Jiangmen 529020, People’s Republic of China

<sup>3</sup> Laboratory of Condensed Matter Spectroscopy and Opto-Electronic Physics, Key Laboratory of Artificial Structures and Quantum Control (Minister of Education), Department of Physics, Shanghai Jiao Tong University, 800 Dong Chuan Road, Shanghai 200240, People’s Republic of China

[13]. However, few studies are done on detailed investigation on the temperature dependence of the phonon behavior in Cu-doped ZnO [14], in contrast to the comprehensive analysis of temperature effects on Raman scattering for other ternary alloys [15, 16]. The substitution of Cu ions at Zn ion sites in ZnO may breakdown the translational symmetry because of the modifications of the crystal lattice, and thus, the information of phonon decay is an essential aspect to understand the lattice dynamical behaviors.

In this paper, we synthesize the Cu-doped ZnO nanocombs by a simple catalyst-free chemical vapor deposition method at 750 °C. Furthermore, Raman spectra of Cu-doped ZnO nanocombs have been comprehensively investigated as a function of temperature (83–443 K) with different Cu compositions (0–3.24 %). In order to study the temperature and dopant effects on the  $E_2(\text{high})$  phonon mode in the Cu-doped ZnO nanocombs, we employ a theoretical model to accurately describe the Raman downshift and linewidth broadening. It is found that the anharmonic effects are enhanced with the increase in Cu dopants and temperature for the  $E_2(\text{high})$  phonon mode. In addition, we will also demonstrate the anharmonic effect on the Raman frequency, linewidth, and lifetime.

## 2 Experimental details

Cu-doped ZnO nanocombs were grown on Si substrate in a horizontal tube furnace by a simple thermal evaporation method. A mixture of Zn powders (99.99 % purity) and  $\text{CuCl}_2$  (99.99 % purity) powders was loaded into an alumina boat, which were placed at the center of a horizontal quartz tube. Then, carefully cleaned n-type Si (100) substrates were placed about 10 cm away from the evaporation source along the downstream position of the carrier gas. By a mechanical rotary pump to remove the residual oxygen, the quartz tube was evacuated to  $\sim 2$  Pa before heating. Next, the carrying gas mixed with  $\text{O}_2$  (flow rate of 50 sccm) and Ar (flow rate of 300 sccm) was introduced from one end of the quartz tube after the furnace was heated to 750 °C at a rate of 10 °C/min. The evaporation was performed at 750 °C for an hour. After the experiment was over, the furnace was cooled naturally to room temperature. Finally, the Cu-doped ZnO nanocombs have been successfully obtained. The prepared samples displayed the light yellow surface layer on the Si substrate. Temperature-dependent micro-Raman scattering spectra were performed in a backscattering geometry of  $z(x, -)\bar{z}$  configuration using a high-resolution Jobin–Yvon LabRAM HR 800UV system. The 514.5-nm line of an Ar ion laser was focused on four samples (a laser spot size of  $\sim 1.3$   $\mu\text{m}$ ) by a 50 $\times$  optical microscopy objective with a numerical aperture of

0.5 yielded. A PHI Quantum 2000 X-ray photoelectron spectroscopy (XPS) (Chanhassen, MN, USA) was employed to measure the bonding characteristics. The morphologies of Cu-doped ZnO nanocombs were obtained by field emission scanning electron microscopy (FE-SEM) (Philips XL30FEG).

## 3 Results and discussion

Figure 1a displays the room-temperature Raman spectra of four Cu-doped ZnO nanocombs with different Cu contents. We have assigned the modes at  $\sim 437$   $\text{cm}^{-1}$  [the sharp Raman peaks],  $\sim 330$ ,  $\sim 384$ , and  $580$   $\text{cm}^{-1}$  to the  $E_2$  (high) phonon modes, the second-order acoustic mode,  $A_1$  transverse optical mode, and  $E_1$  longitudinal optical mode, respectively [17]. These phonon behaviors are characteristics of Cu-doped ZnO nanocombs, which will provide much physical information on the alloy disorder effect and electronic state localization [3]. It is noted that the  $E_2(\text{high})$  phonons shift to lower frequency and asymmetrically broaden as the Cu composition increases. In addition, an additional mode near  $534$   $\text{cm}^{-1}$  is found in the Cu-doped ZnO nanocombs, which can be attributed to the substitutional incorporation of Cu ions into the host ZnO lattice [18]. Moreover, the intensity of the additional mode enhances with the Cu composition increasing, indicating that more lattice defects triggered by Cu doping are introduced in Cu-doped ZnO samples. As an example, Fig. 1b presents the XPS spectra of Cu-doped ZnO (1.17 %), and the inset shows the typical FE-SEM image of

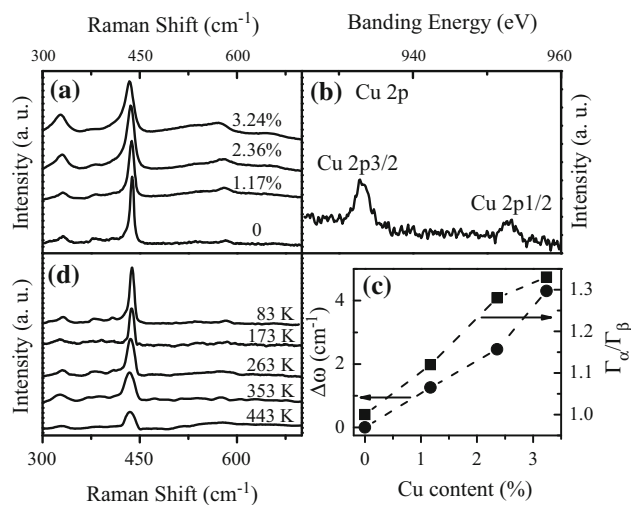


**Fig. 1** **a** Room-temperature spectra of Cu-doped ZnO with different Cu compositions, **b** XPS of Cu 2p for Cu-doped ZnO (1.17 %) nanocombs, together with the corresponding SEM pattern shown in the inset, **c** asymmetry  $\Gamma_\alpha/\Gamma_\beta$  and Raman shift  $\Delta\omega$  of the  $E_2(\text{high})$  phonon mode versus Cu content, **d** temperature-dependent Raman spectra of Cu-doped ZnO (1.17 %) nanocombs

the corresponding sample. The peaks of Cu 2p<sub>3/2</sub> (933.1 eV) and Cu 2p<sub>1/2</sub> (952.5 eV) demonstrate that Cu ions are a bivalent state in Cu-doped ZnO nanocombs [19]. That is consistent with room-temperature Raman spectra of Cu-doped ZnO nanocombs (Fig. 1a).

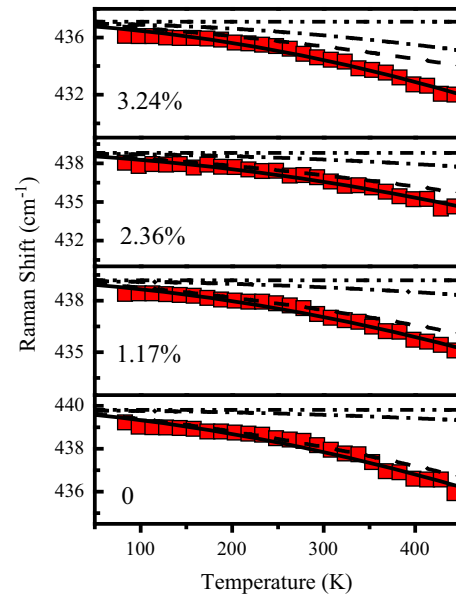
Figure 1c exhibits the asymmetric ratio  $\Gamma_\alpha/\Gamma_\beta$  (solid squares) and the frequency shift  $\Delta\omega$  from that of pure ZnO nanocombs (solid circles) as a function of Cu content, where  $\Gamma_\alpha$  ( $\Gamma_\beta$ ) is defined as the low-frequency (high-frequency) half width at half maximum in the phonon line. The asymmetric ratio  $\Gamma_\alpha/\Gamma_\beta$  and the frequency shift  $\Delta\omega$  of the  $E_2(\text{high})$  phonon increase with the increasing of Cu content. This result comes from the alloy potential fluctuation, since not only topological disorder but also structural disorder is induced by atom substitution in ternary alloys [12, 20]. As a result, the disorders break the translational symmetry, leading to the contribution of  $q \neq 0$  phonons to the Raman line shape. In order to accurately calculate the frequency shift and linewidth of  $E_2$  phonon modes, we have employed spatial correlation model (SCM) to fit the Raman spectra of  $E_2(\text{high})$  phonon mode in different temperatures. Figure 1d shows the temperature dependence of Raman spectra of the  $E_2(\text{high})$  phonon mode in the Cu-doped ZnO nanocombs with 1.17 % Cu composition in the range from 83 to 443 K. It is found that the  $E_2(\text{high})$  phonon peak broadens and shifts to lower frequency with increasing temperature. In the following, we mainly focus on the changes of the Raman shift, linewidth, and lifetime of the  $E_2(\text{high})$  mode in Cu-doped ZnO nanocombs with temperature.

Figure 2 shows the Raman frequencies of the  $E_2(\text{high})$  mode as a function of the temperature for four Cu-doped ZnO nanocombs. The Raman frequency decreases with increasing temperature, because of the thermal expansion of the lattice and the anharmonic coupling of the phonon. Including the temperature-dependent peak position, the Raman frequency  $\omega(T)$  can be shown as [21]:

$$\omega(T) = \omega_0 + \Delta\omega_1(T) + \Delta\omega_2(T) \tag{1}$$

where  $\omega_0$  is the harmonic frequency,  $\Delta\omega_1(T)$  is the frequency shift due to the thermal expansion of the lattice and can be written as  $\Delta\omega_1(T) = -\omega_0\gamma \int_0^T [\alpha_c(T') + 2\alpha_a(T')]dT'$ , with  $\gamma$  the Grüneisen parameter [22],  $\alpha_c$  and  $\alpha_a$  the parallel and perpendicular temperature-dependent coefficients of linear thermal expansion of ZnO, respectively [23].  $\Delta\omega_2(T)$  is the frequency shift due to phonon decay processes.

The phonon decay term  $\Delta\omega_2(T)$  depicts the anharmonic coupling between phonons. Considering the anharmonic phonon coupling to two phonons (three-phonon process) and three phonons (four-phonon coupling), it can be given by [21]



**Fig. 2** Measured Raman shifts of the  $E_2(\text{high})$  phonon mode in Cu-doped ZnO nanocombs with different Cu compositions as a function of temperature. The experimental values are shown as the *solid squares*. The *solid curves* display the theoretical calculation results relating the contributions from the different terms in Eqs. (1) and (2), respectively, with  $\omega_0$  (*dashed-dot-dotted curves*),  $\omega_0 + \Delta\omega_1$  (*dashed-dot curves*),  $\omega_0 + \Delta\omega_2$  (*dashed curves*)

$$\Delta\omega_d(T) = A \left( 1 + \frac{2}{e^{(\hbar\omega_0/2k_B T)} - 1} \right) + B \left( 1 + \frac{3}{e^{(\hbar\omega_0/2k_B T)} - 1} + \frac{3}{(e^{(\hbar\omega_0/2k_B T)} - 1)^2} \right) \tag{2}$$

The anharmonic constants  $A$  and  $B$  are related to the relative probability of the occurrence of each process and taken as fitting parameters to the experimental data. However, the  $E_2(\text{high})$  phonon cannot decay into two longitudinal acoustic (LA) or transverse acoustic (TA) phonons of equal frequency and opposite wave vector in the three-phonon process for ZnO, since one half of the  $E_2(\text{high})$  phonon energy is less than the energy gap between the acoustic and optical phonon branches ( $\omega_{E_2(\text{high})} < 2\omega_{\text{LA,TA}}$ ) [22]. On the other hand,  $E_2(\text{high})$  phonon is located at the lower edge of the optical phonon branch, so it also cannot decay into a transverse optical (TO) phonon and a TA (LA) phonon. In consequence, we only need to take into account the four-phonon process for the fitting of the decay of the  $E_2(\text{high})$  phonon in Cu-doped ZnO nanocombs with the symmetric decay of zone-center phonons into three phonons to the frequency  $\omega_0/3$ , respectively. The solid curves in Fig. 2 are the calculated phonon frequencies with an increase in temperature using Eqs. (1) and (2). The fitting parameters  $\omega_0$  and  $B$  are given

**Table 1** Fitting parameters for the Raman frequencies, linewidths, and lifetimes of the  $E_2(\text{high})$  phonon mode of Cu-doped ZnO nanocombs

Cu content	$\omega_0$ (cm <sup>-1</sup> )	$B$ (cm <sup>-1</sup> )	$\Gamma_0$ (cm <sup>-1</sup> )	$C$ (cm <sup>-1</sup> )	$\tau_{\text{anharmonic}}$ (ps)		
					83 K	308 K	433 K
0	439.81	-0.011	4.31	0.31	1.70	0.65	0.29
1.17 %	439.19	-0.034	6.05	0.39	1.66	0.64	0.28
2.36 %	438.99	-0.096	10.25	0.40	1.64	0.63	0.28
3.24 %	438.90	-0.137	12.11	0.55	1.58	0.60	0.26

in Table 1 in the case of different Cu compositions. We note that the results of theoretical analysis agree well with the experiments of the Raman shift with an increase in temperature under different Cu compositions. In order to distinguish the contributions of the lattice thermal and anharmonic decay effect for the Raman shift, we have also presented the net contribution of  $\Delta\omega_1(T)$  and  $\Delta\omega_2(T)$  in Fig. 2. It is noted that the anharmonic decay to other phonons is mainly responsible for the Raman frequency downshift through four-phonon processes with low Cu composition, especially in the high-temperature range. However, the lattice thermal process also plays a key role in the Raman frequency downshift with high Cu composition (3.24 %).

Several factors, involving the finite resolution of the spectrometer [24], the alloy-induced disorder, and the anharmonic decay of the phonon [25], all contribute to the linewidth broadening  $\Gamma(T)$  of the Raman peaks, whereas the finite resolution of the spectrometer and alloy-induced disorder induced the phonon linewidth broadening, which are not dependent on the temperature. Although the lattice thermal expansion is leading to the Raman frequency shift, it is not responsible for the broadening of the phonon peaks. Therefore, the pure anharmonic broadening mainly results in the decay into lower-energy phonons for the temperature-dependent phonon linewidth. Similar to the temperature-dependent Raman frequency, the phonon linewidth can be expected by the assumption of the asymmetric decay into two phonons with frequencies  $\omega_1$  and  $\omega_2$  and symmetric decay into three phonons with frequency  $\omega_0/3$ . According to the above analysis, the asymmetric two-phonon decay process will not occur for the  $E_2(\text{high})$  phonon mode in Cu-doped ZnO nanocombs, and thus, the temperature-dependent phonon linewidth  $\Gamma(T)$  can be described by [21]:

$$\begin{aligned} \Gamma(T) &= \Gamma_0 + \Gamma_{\text{anharmonic}} \\ &= \Gamma_0 + C \left( 1 + \frac{3}{e^{(\hbar\omega_0/2k_B T)} - 1} + \frac{3}{(e^{(\hbar\omega_0/2k_B T)} - 1)^2} \right) \end{aligned} \quad (3)$$

where  $\Gamma_0$  is attributed to inherent defect or impurity scattering. The second term represents the symmetric decay of four-phonon process. Anharmonic constant  $C$  is related to the probability of the occurrence of this process. Figure 3a

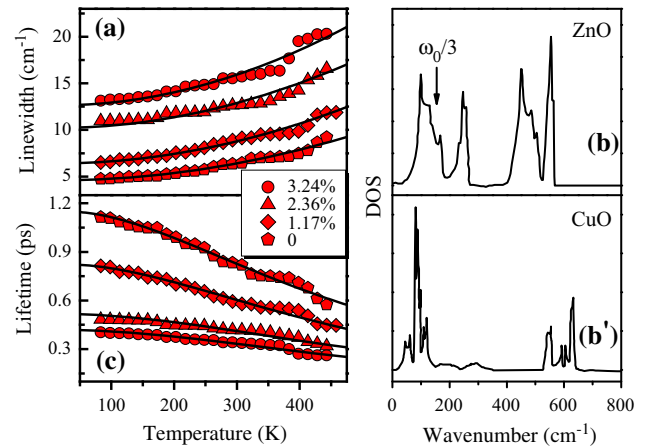


**Fig. 3** **a** Measured Raman linewidths of the  $E_2(\text{high})$  phonon mode in Cu-doped ZnO nanocombs with different Cu compositions as a function of temperature. The *solid curves* display the theoretical calculation results with Eq. (3). **b** The calculated phonon DOS of pure ZnO recorded in Ref. [22], and **b'** the calculated phonon DOS of CuO recorded in Ref. [27]. The position of  $\omega_0/3$  is marked by an *arrow*. **c** Lifetime  $\tau(T)$  of the  $E_2(\text{high})$  phonon mode of Cu-doped ZnO with different Cu compositions as a function of temperature. The *solid curves* are the theoretical calculation results with Eq. (4)

displays the temperature-dependent linewidths of the  $E_2(\text{high})$  phonon mode in Cu-doped ZnO nanocombs using the least-square fit of Eq. (3) (*solid curves*). The fitting parameters  $\Gamma_0$  and  $C$  are also presented in Table 1.

It is worth noting that the value of  $\omega_0$  varies with Cu composition, which can be ascribed well to the variation of the lattice constant. Due to the incorporation of Cu substitutionally into the Zn sublattice, the lattice constants of ZnO increase with the increasing in Cu composition [26], leading to the decrease in  $\omega_0$ . Furthermore, we can also clearly observe that the anharmonic constants  $B$  and  $C$  of the  $E_2(\text{high})$  phonon mode in Cu-doped ZnO alloys are bigger than that in pure ZnO nanocombs, as given in Table 1. In Cu-doped ZnO, the increasing impurity-induced disorder with the Cu composition gives rise to an increase in phonon density of states (DOS), resulting in an increase in the probability of inelastic (anharmonic) scattering between phonons and the substitutional atoms. In addition, such a behavior is consistent with the calculated phonon DOS of ZnO given by Serrano et al. (as shown in Fig. 3b) [22], where the intensity of  $\omega_0/3$  ( $\sim 147$  cm<sup>-1</sup>) increases with the decreasing of  $\omega_0$ , indicating an

increasing of the occurrence probability of four-phonon process. Moreover, the decreasing of  $\omega_0$  with Cu composition also results in an increase in the phonon DOS in Cu-doped ZnO due to the increasing CuO phonon DOS (the lowest intensity at  $\sim 150 \text{ cm}^{-1}$ ) (as shown in Fig. 3b) [27]. As a consequence, the anharmonic constants due to impurity-induced disorder enhance with the increase in Cu composition. On the other hand, the increasing temperature produces larger numbers of phonons, which also result in an increase in probability in inelastic (anharmonic) scattering between phonons and the substitutive atoms [15]. The probability of inelastic decay of phonons will become bigger with the increasing number of the substitutive atoms. Therefore, the impurity-induced disorder anharmonicity is quite obvious by an increase in temperature in these Cu-doped ZnO nanocombs.

Finally, it is well known that the linewidth broadening is usually connected with the lifetime  $\tau(T)$  of the decay processes of the involved phonons. The estimated relaxation time can be written by [15, 21]:

$$\frac{1}{\tau} = \frac{1}{\tau_{\text{elastic}}} + \frac{1}{\tau_{\text{anharmonic}}}, \quad (4)$$

where  $\tau_{\text{elastic}} = 1/(2\pi c\Gamma_0)$  is closely related to the elastic scattering, and  $\tau_{\text{anharmonic}} = 1/(2\pi c\Gamma_{\text{anharmonic}})$  is relation to the anharmonic decay, with  $c$  the velocity of light. Figure 3c exhibits the lifetimes  $\tau(T)$  of the  $E_2(\text{high})$  mode in Cu-doped ZnO nanocombs with different Cu compositions as a function of temperature, and the solid curves are the theoretical fitting results. The anharmonic decay time ( $\tau_{\text{anharmonic}}$ ) of the  $E_2(\text{high})$  phonon mode in Cu-doped ZnO nanocombs is also listed in Table 1. It is significant that the lifetime of the  $E_2(\text{high})$  mode becomes shorter with an increase in Cu composition and lattice temperature. It is reasonable and understandable that the phonon mean free path decreases with the increase in temperature due to the thermal interaction, while the anharmonicity due to disorder further enhances the decay of the  $E_2(\text{high})$  mode in Cu-doped ZnO.

## 4 Conclusions

In summary, temperature-dependent Raman spectra have been investigated in detail under the temperature range from 83 to 443 K for the Cu-doped ZnO nanocombs with different Cu compositions (0–0.324 %), grown by a simple catalyst-free chemical vapor deposition method. By the aid of SCM model, We obtain the phonon frequencies and linewidths of the  $E_2(\text{high})$  mode in Cu-doped ZnO nanocombs throughout the temperature ranges (83–443 K). A statistical model involves the contributions of the thermal expansion, and symmetric four-phonon coupling has been employed to fit

the temperature-dependent frequencies and linewidths. We have explained in detail that the frequency shift and linewidth of  $E_2(\text{high})$  phonon mode vary sensitively with temperature and Cu composition in Cu-doped ZnO nanocombs. Due to the variation in the lattice structure and phonon density of states in Cu-doped ZnO, we can find that the contribution of anharmonic effects of the four-phonon process enhances with the increase in Cu composition.

**Acknowledgments** This work was supported by the Innovation Project of Department of Education of Guangdong Province (No. 2014KTSCX131).

## References

1. H. Ohno, *Science* **281**, 951 (1998)
2. L.H. Ye, A.J. Freeman, B. Delley, *Phys. Rev. B* **73**, 165424 (2006)
3. D.B. Buchholz, R.P.H. Chang, J.H. Song, J.B. Ketterson, *Appl. Phys. Lett.* **87**, 082504 (2005)
4. T.S. Heng, S.P. Lau, S.F. Yu, J.S. Chen, K.S. Teng, *J. Magn. Mater.* **315**, 107 (2007)
5. S. Karamat, R.S. Rawat, T.L. Tan, P. Lee, S.V. Springham, M. Anis-ur-Rehman, R. Chen, H.D. Sun, *J. Supercond Nov. Magn.* **26**, 187 (2013)
6. W. Dai, X.H. Pan, C. Chen, S.S. Chen, W. Chen, H.H. Zhang, Z.Z. Ye, *RSC Adv.* **4**, 31969 (2014)
7. N.A. Shan, M. Abid, M. Amin, R. Afrin, S.Z. Ilyas, *Sens. Transducers J.* **186**, 3 (2015)
8. G.Z. Xing, G.C. Xing, M.J. Li, E.J. Sie, D.D. Wang, A. Sulistio, Q.L. Ye, C.H.A. Huan, T. Wu, T.C. Sum, *Appl. Phys. Lett.* **98**, 102105 (2011)
9. M. Balkanski, R.F. Wallis, E. Haro, *Phys. Rev. B* **28**, 1928 (1983)
10. P.G. Klemens, *Phys. Rev.* **148**, 845 (1996)
11. T.R. Hart, R.L. Aggarwal, B. Lux, *Phys. Rev. B* **1**, 638 (1970)
12. J.B. Wang, H.M. Zhong, Z.F. Li, W. Lu, *J. Appl. Phys.* **97**, 086105 (2005)
13. H. Fujimori, H. Komatsu, K. Ioku, S. Goto, M. Yoshimura, *Phys. Rev. B* **66**, 064306 (2002)
14. J.L. Yu, Y.F. Lai, S.Y. Cheng, Q. Zheng, Y.H. Chen, *J. Lumin.* **161**, 330 (2015)
15. H.F. Liu, N. Xiang, S. Tripathy, S.J. Chua, *J. Appl. Phys.* **99**, 103503 (2006)
16. L.B. Jiang, H. Li, S.B. Zuo, H.Q. Bao, W.J. Wang, X.L. Chen, *Appl. Phys. A* **100**, 545 (2010)
17. B.Q. Cao, W.P. Cai, H.B. Zeng, G.T. Duan, *J. Appl. Phys.* **99**, 073516 (2006)
18. T.L. Phan, R. Vincent, D. Cherns, N.X. Nghia, V.V. Ursaki, *Nanotechnology* **19**, 475702 (2008)
19. D.Q. Gao, Y. Xu, Z.H. Zhang, H. Gao, D.S. Xue, *J. Appl. Phys.* **105**, 063903 (2009)
20. P. Parayanthal, F.H. Pollak, *Phys. Rev. Lett.* **52**, 1822 (1984)
21. X.D. Pu, J. Chen, W.Z. Shen, H. Ogawa, Q.X. Guo, *J. Appl. Phys.* **98**, 033527 (2005)
22. J. Serrano, A.H. Romero, F.J. Manjón, R. Lauck, M. Cardona, A. Rubio, *Phys. Rev. B* **69**, 094306 (2004)
23. H. Iwanaga, A. Kunishige, S. Takeuchi, *J. Mater. Sci.* **35**, 2451 (2000)
24. P. Verma, S.C. Abbi, K.P. Jain, *Phys. Rev. B* **51**, 16660 (1995)
25. H.H. Burke, I.P. Herman, *Phys. Rev. B* **48**, 15016 (1993)
26. R.D. Shannon, *Acta Crystallogr. A* **32**, 751 (1976)
27. M.M. Beg, S.M. Shapiro, *Phys. Rev. B* **13**, 1728 (1976)